City Research Online

City, University of London Institutional Repository

Citation: Grattan, K. T. V. & Rahman, B. M. (2022). Temperature-independent Vibration Sensor Based on Fabry-Perot Interferometer using a Fiber Bragg Grating approach. Optical Engineering,

This is the accepted version of the paper.

This version of the publication may differ from the final published version.

Permanent repository link: https://openaccess.city.ac.uk/id/eprint/27741/

Link to published version:

Copyright: City Research Online aims to make research outputs of City, University of London available to a wider audience. Copyright and Moral Rights remain with the author(s) and/or copyright holders. URLs from City Research Online may be freely distributed and linked to.

Reuse: Copies of full items can be used for personal research or study, educational, or not-for-profit purposes without prior permission or charge. Provided that the authors, title and full bibliographic details are credited, a hyperlink and/or URL is given for the original metadata page and the content is not changed in any way.

City Research Online: http://openaccess.city.ac.uk/ publications@city.ac.uk

Temperature-independent Vibration Sensor Based on Fabry-Perot Interferometer using a Fiber Bragg Grating approach

Abstract

An innovative vibration sensor based on a Fabry-Perot Interferometer (FPI) using Fiber Bragg Grating (FBG) reflectors has been discussed in this work. The sensor has been designed to be compact and easy to fabricate and independent of temperature, to overcome limitations seen in some previous designs, providing an effective correction for temperature effects in FBG-based FPI (FBG-FPI) sensors. In this approach, light from a broadband source in the wavelength range 1500 – 1580 nm has been used to illuminate the FBGs used (having a reflective peak of 1547.42 nm), employing in this way a light source within the FPI optimum wavelength operating range of 1547.15 nm – 1547.80 nm. The sensor developed in this work has been shown able to capture a 3 kHz burst signal from a signal generator, in 1 Hz, 2 Hz, and 3 Hz intervals. In addition, the research carried out has revealed that the sensor could be used to capture sinusoidal signals at frequencies up to 9 kHz, creating a performance comparable with many existing conventional piezoelectric sensors. The ability to operate regardless of any ambient temperature changes (in the range from 26.5°C (room temperature) up until 80°C), opens the way to use such a sensor system over a wide range of engineering applications taking advantage of the next generation of FBG-based FPIs.

1. Introduction

Vibration measurement is of critical concern in many current engineering applications and excessive vibration or vibration at particular frequencies can have series of effects on the performance and indeed the safety of many engineering structures, such as aircraft or buildings. Hence, accurate measurement and monitoring must be done precisely and easily, to allow the detection of anomalous events and to warn of potential infrastructure damage [1]. Vibration sensors based on piezoelectric [2,3], magnetostrictive [4], capacitive [5], and inductive [6] technologies, among others, are already available and widely used by engineers in the industry. However, there are problems for many important applications – traditional vibration sensors suffer from electromagnetic (EM) interference, making them unsuitable when applied to many challenging situations and electrical sensors may be unsuitable for use in certain safety-critical areas e.g. where explosive or flammable gases are present. Furthermore, with the developing needs in modern engineering measurement, there is a requirement for new designs that can

overcome limitations of the monitoring distance experienced experienced in some applications (e.g. civil infrastructure), as well as the expensive maintenance costs required for some designs of sensor systems.

Optical fiber-based systems offer new opportunities for better sensor design and these have received significant attention in research, to address a wide range of applications over the last several decades, taking advantage of their being lightweight, operational over significant lengths (through multiplexing of the sensors along with the optical network), potentially high accuracy, having good signal transmission security and due to their configuration, relatively easy installation, as well as corrosion resistance (not being metallic) and immunity to electromagnetic (EM) interference [7,8]. These features emphasize their potential to be used in harsh environments in the industry [9] where conventional sensors may often be limited. Building on the low cost of many fiber optic components (due to their widespread use in telecommunications), these are well suited to many different areas of optical fiber sensing, with key examples already proven being strain sensors [10–12], temperature sensors [13,14], and vibration sensors [15,16], often showing high sensitivity [17].

A fiber optic vibration sensor can typically be based on the modulation of the light properties in the optical fiber, such as intensity, phase, polarisation state, and frequency, where these are (mainly) caused by externally applied vibration (and compensation for extraneous effects such as temperature can be included). The most common types of fiber-optic vibration sensors discussed in the literature are point [18–21], quasi-distributed [22], and distributed sensors [23,24] and for each of those different (and often complementary) optical techniques can be employed. For vibration measurement, several point sensor schemes such as those based on Fiber Bragg Gratings (FBGs), Fabry–Pérot interferometers [25,26], self-mixing of optical signals [27], and Doppler vibrometry [28,29] have been reported in the literature. Because of inherent features of the optically-based technique such as low noise, ease of being embedded in a structure and the ability readily to be multiplexed to form a quasi-distributed sensor array, FBG vibration sensors have become a rapidly growing scientific research topic [30,31] to meet the range of new engineering applications, both current and under development, where better vibration measurement is needed.

Amongst the wide range of FBG-based sensors that have already been proposed, relatively few FBG-based Fabry-Perot Interferometer (FPI) sensors have been discussed in the literature [32–35]. Amongst these, Wada et al. [32,33] used a tunable laser diode to illuminate the FBG-FPI sensor, subjected to a sinusoidal vibration. In addition, Zaini et al. [35] have used an edge filter interrogation method, where a further FBG-FPI was included to filter the output

signal from the FBG-FPI used as the sensor. In these designs in the literature [32,33,35], while an effective FBG-FPI based vibration sensor has been developed, the designs proposed did not include an explicit temperature compensation scheme. Rao et al. [34] have discussed an FBG-FPI based design to monitor strain, temperature, and vibration simultaneously and although in that work the FBG-based sensor was used from room temperature to 50°C, temperature effects were not fully eliminated when making vibration measurements using this FBG-based approach.

Seeking to overcome some of these limitations in this work, a temperature-independent vibration sensor using a Fabry-Perot interferometer approach and based on FBG technology has been developed and its performance is described. This new sensor approach can detect burst signals, at low frequencies and can find applications in areas such as ground/slope monitoring and structural vibrations as in structural health monitoring. The target performance specification of the sensor design proposed was to detect a ~3kHz burst at 1Hz, 2Hz, and 3Hz frequencies, doing so over a range of temperatures and compensating for any temperature effects. The results obtained have shown that the sensor can monitor sinusoidal signals, at frequencies up to ~9kHz, achieving temperature compensation in the detection of low-frequency burst signals and high-frequency sinusoidal waves, in this way creating a sensor scheme that potentially addressed important sensing needs for the next generation of FBG-based FPI devices.

2. Methodology

2.1 Fabrication of the Fiber Bragg Gratings (FBGs).

The FBGs used in this study were created by inscribing uniform gratings in the core of conventional single-mode fiber (SMF), using the phase mask technique. Before this, the optical fiber was sensitized by hydrogen-loading the SMF used, in a high-pressure hydrogen environment, for five days. Following that, the gratings were inscribed at a length of ~10 mm inside the fiber core, by using light from a Krypton Fluoride (KrF*) excimer laser, operating at a wavelength of 248 nm. The fiber samples containing the inscribed gratings were heated in an oven at 70°C to 80°C for typically seven hours, after the production procedure was completed, to remove any remaining hydrogen present as to stabilize the gratings.

For every FBG inscribed in a single-mode fiber (SMF), the shift of the Bragg wavelength can be linearly related with the change of strain, ε, and temperature, T, as described by the following relationship:

$$\frac{\Delta\lambda_B}{\lambda_B} = (1 - p_{eff})\Delta\varepsilon + (\alpha + \xi)\Delta T$$

where λ_B represent the Bragg wavelength, while p_{eff}, α, and ξ are for the photo-elastic parameter, thermal expansion coefficient, and thermo-optic coefficient of the fiber, respectively.

2.2 Fabrication of in-fiber FPI

In a way that is similar to the fabrication of the FBGs themselves, the in-fiber FPI was formed by using two identical gratings, forming extremely narrow fringes that were linearly shifted with the change of temperature and strain applied to the FBG-FPI. The two short uniform gratings formed the in-fiber FBG-FPI, is illustrated in Fig. 1, using equal grating lengths, L_{FBG}, and grating period, Λ wrote into an optical fiber, as shown. This FBG-FPI has two gratings, separated by a known distance, L_{FPI}, to produce the interferometric spectra. Fig. 2(a) shows the reflection spectra of an individual grating reflector (a single grating FBG, operating at a specific known wavelength, λ). The bare fiber between the two grating reflectors creates the cavity for the resonating optical wave between the two reflectors, producing the interferometric output spectra, as illustrated in Fig. 2(b).

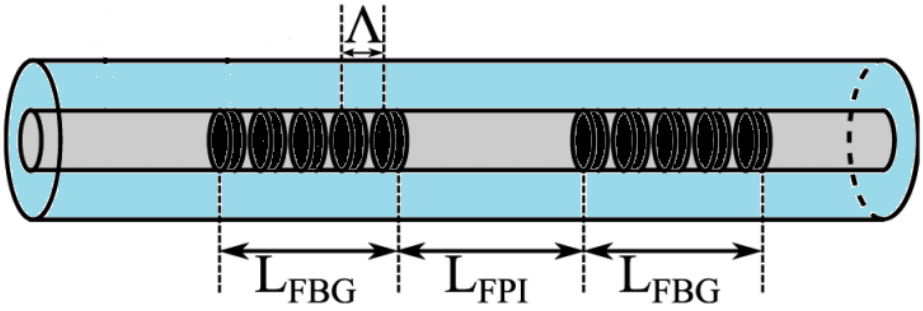

Fig. 1 Illustration of the FBG-FPI created in this work where L_{FBG} is the length of the grating used (of period Λ) and L_{FPI} is the separation of the gratings, and thus the interferometric cavity length.

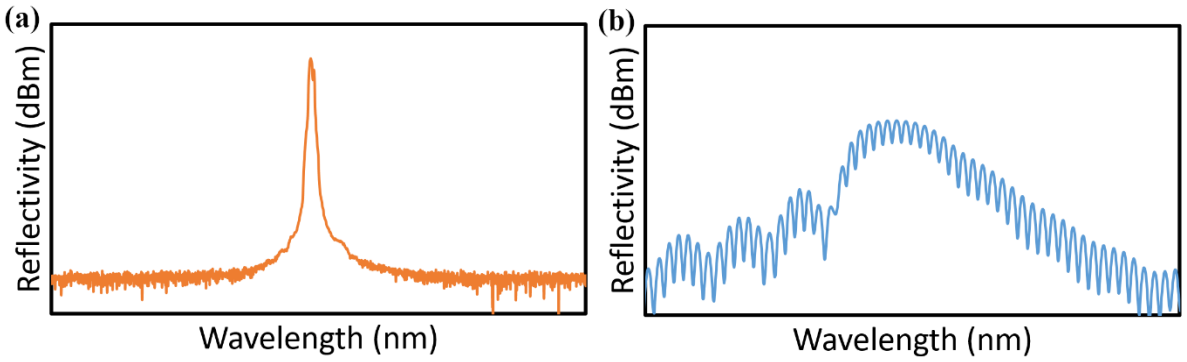

Fig. 2. Illustrations of (a) a single FBG spectrum, of wavelength λ and (b) a typical spectrum of the FBG-FPI.

2.3 Experimental Design

The experimental setup used is illustrated in Fig. 3, where two types of the sensor were used – the first being a 'normal' FBG with a reflection peak wavelength of 1547.42 nm, while the second was an FBG-based Fabry-Perot interferometer (denoted as FBG-FPI) with an optimum operating wavelength range of 1547.15 nm – 1547.80 nm. Light from a broadband source over the range 1500 – 1580 nm was passed through the normal FBG before being connected to Port 1 of a 3-port optical circulator. In the design of the FBG-FPI, these two gratings must be spaced closely together and have the same range of wavelength peak (or at least to be so within ~0.1 nm). The standard grating will act as a filter for the broadband source and only allow light at a particular wavelength (the same wavelength peak as for the FBG-FPI) to pass through. The sensitivity of the FBG-FPI would be negatively affected if the wavelength of the light source did not match the optimum operating range of the FBG-FPI: indeed, a severe mismatch would render the sensor ineffective. Moreover, as the FBG responds directly to strain and temperature variations, when the surrounding temperature changes, the wavelength shift for the normal FBG used will be identical to that of the FBG-FPI cavity, formed from the two FBGs and in that way deal with the temperature compensation needed. In the experiment carried out, Port 2 of the circulator was connected to the FBG-FPI cavity to detect the waveforms generated. Following that, a piezoelectric transducer was placed on top of the FBG-FPI, separated from it by a 2x2x0.1 mm plastic sheet, illustrating a scenario where seismic activity will be detected. Port 3 was connected to the DLM2054 2.5 G/s 500 MHz oscilloscope, through a DET02AFC photodetector, to capture the response of the FBG-FPI in the detection of the applied vibration.

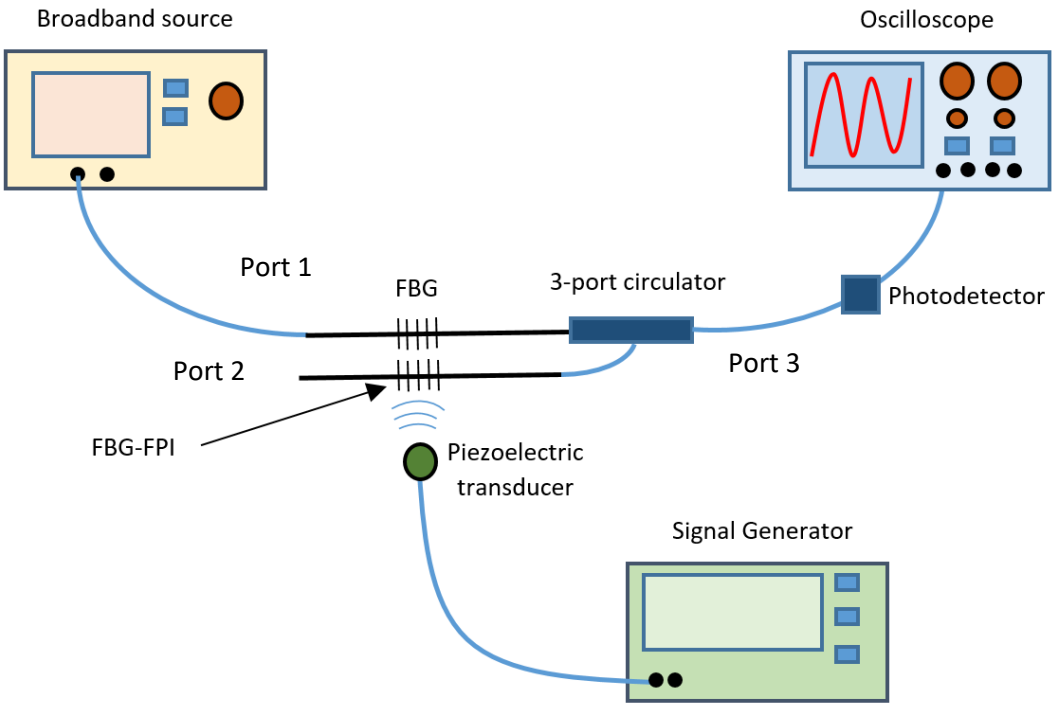

Fig. 3. Illustration of the experimental setup for the verification of the performance of the FBG-FPI cavity subjected to a simulated seismic-induced vibration

The output spectra obtained from the setup shown in Fig. 3 are illustrated in Fig. 4, obtained by connecting an Optical Spectrum Analyzer (OSA) to Port 3 of the circulator instead of the oscilloscope. As indicated above, the FBG peak (1547.42 nm) is within the optimum operating range of the FBG-FPI (1547.15 – 1547.80 nm).

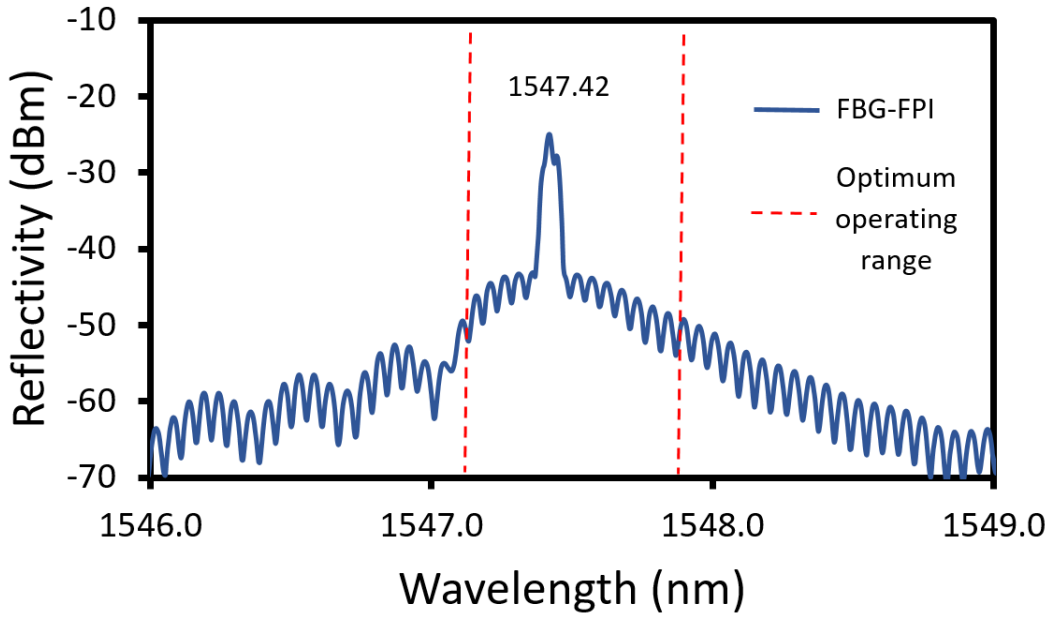

Fig. 4. The output spectrum of FBG and FBG-FPI from Port 3 of the circulator when connected to an Optical Spectrum Analyzer.

2.4 Burst Signal in Low-Frequency Interval

With reference to Fig. 3, a 0.5 V peak-to-peak voltage (V_{pp}) 3 kHz burst signal from the ROHDE & SCHWARZ RTM3004 signal generator was applied to the FBG-FPI, using a piezoelectric transducer where the frequency of the burst interval was varied from 1 Hz, 2 Hz, and 3 Hz.

2.5 High Frequency of Sinusoidal Wave

Using the same setup as discussed above, a 3 kHz sine wave with 5 V_{pp} from the signal generator was applied to the FBG-FPI through the piezoelectric transducer. The input frequency was varied up to a maximum of 9 kHz, in 1 kHz intervals. To allow a cross-comparison, the experiment was repeated using a conventional piezoelectric sensor to compare the performance characteristics of the two approaches used to monitor vibration.

2.6 Temperature Monitoring and creating a correction for temperature effects

The procedures above were carried out by placing the experimental setup on a hot plate to investigate the effect of temperature on the FBG-FPI sensor. Due to the small size of the device illustrated schematically in Fig. 1, as the wavelength shifts due to the temperature of the FBGs used are the same for each, there should then be no changes in the ability of the FBG-FPI to operate as an interfometer and thus capture the vibration waveforms (generated in this test by the signal generator at known frequencies). An illustration of the experiment setup used for calibration of the system is shown in Fig. 5, where both the FBGs and the FPI were placed on top of a hot plate and between the piezoelectric transducer. Here a thermocouple was utilized in this calibration to monitor the temperature of the hot plate, which when it was raised from ~26°C to 80°C in 10°C intervals, the wavelength spectrum of the FBG-FPI from port 3 of the circulator was observed and recorded by using the OSA. Such a calibration is a pre-condition to the use of the sensor system for vibration monitoring and as the FPI continues to work well over this temperature range, shows that the wavelength shift of both gratings (due to changes in the temperature) is essentially identical (with a sensor of this small size).

Thus the procedures set out in Sections 2.4 and 2.5 were repeated over a wide range of temperatures, from room temperature of ~26°C to 80°C, in 10°C intervals. The waveforms captured from the FBG-FPI were recorded from an oscilloscope.

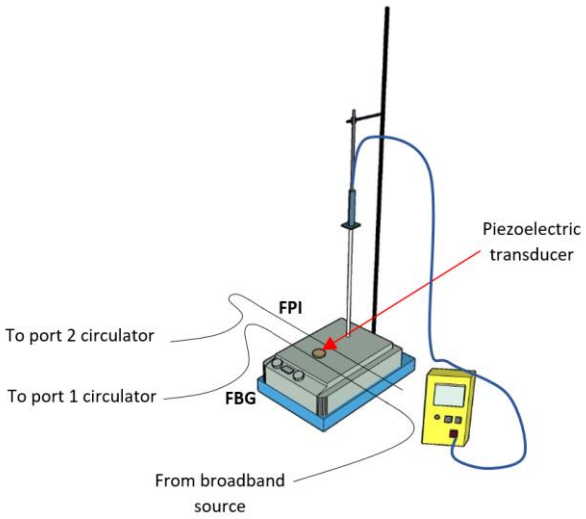

Fig. 5. Experimental set up for the calibration of the FPI sensor over a wide temperature range

3. Results and Discussions

The output signals (generated directly from the signal generator in the system calibration setup used) shown in Fig. 3, are depicted in Fig. 6. Fig. 6(a) shows the 3 kHz burst signal in a 1-second interval (1Hz), and Fig. 6(b) illustrates the 3 kHz sine signal. After being exposed to the 3 kHz burst signal, the responses of the FBG-FPI sensor designed here to the burst signal are shown in Fig. 7. This allows a comparison to be made between the output signal of the signal generator and (what should then be a similar) output signal deteted by the FBG-FPI. Fig. 7(a), (b), and (c) represent the FBG-FPI response to the 3 kHz burst signal in 1 Hz, 2 Hz, and 3 Hz intervals, respectively. As can be seen from Fig. 7, there is minimal background noise in the output reading, primarily due to the suitable nature of the input broadband source [35]. Compared to the output obtained directly from the signal generator (Fig. 6), a small voltage (amplitude) difference between the signal generator output (0.5 V_{pp}) and the FBG-FPI output (~0.2 - 0.3 V_{pp}) was seen, this being due to due to the energy loss experienced. However, the similarity in the structure of the pulses demonstrates that the FBG-FPI can faithfully capture the burst signals used, at low-frequency intervals.

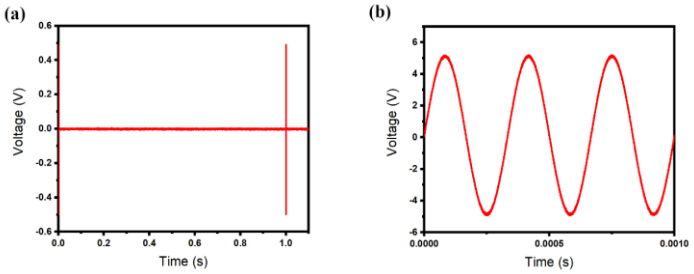

Fig. 6. (a) Signals directly from the signal generator: 3 kHz burst at a 1 Hz interval, and (b) 3 kHz sine wave, generated by the signal generator.

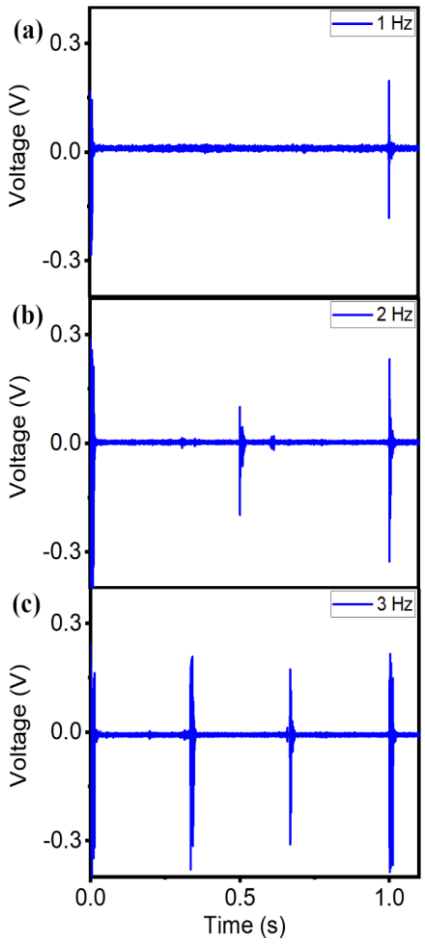

Fig. 7 Illustrating the comparison between the output signal of the signal generator and the output signal from the FBG-FPI: 3 kHz burst at (a) 1 Hz, (b) 2 Hz, and (c) 3 Hz intervals detected by the FBG-FPI.

Fig. 8 now illustrates the response of the piezoelectric sensor, compared to the FBG-FPI when both were subjected to the 3 kHz sine wave from the signal generator. Compared to the 3 kHz output directly from the signal generator in Fig. 6(b), both sensors record an observable loss in input voltage (as elastic waves lose energy as they travel through a material) where in this case a plastic sheet divides the sensor and the transducer (the vibration source). The small distortion is seen in the sine wave of the FBG-FPI output signal (in Fig. 8(b)) seems likely to have been caused by the vibration of the fiber itself – the conventional piezoelectric sensor illustrates the sine wave shape better because the sensor plate was metal (likely aluminum), providing good response to elastic waves. The data show that the FBG-FPI sensor can capture the high-frequency resonance in a similar way to conventional vibration sensors.

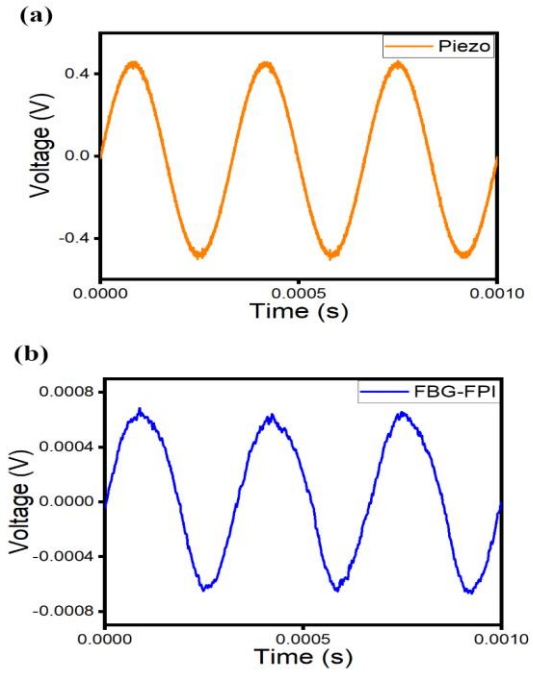

Fig. 8. Output signal detected by (a) the piezoelectric sensor and (b) the FBG-FPI sensor: both were subjected to a similar 3 kHz sine wave.

In addition to the test carried out where the results are illustrated in Fig. 8, a comparison was also made between the output signal directly from the signal generator (SG), the piezoelectric sensor, and the FBG-FPI sensor, as can be seen in Fig. 9. The data shown illustrate the output waveform from each sensor when they were subjected to a sinusoidal wave at a series of frequencies of (a) 3 kHz, (b) 6 kHz, and (c) 9 kHz, where it is evident that FBG-FPI can capture the waveforms in the high-frequency region with high fidelity.

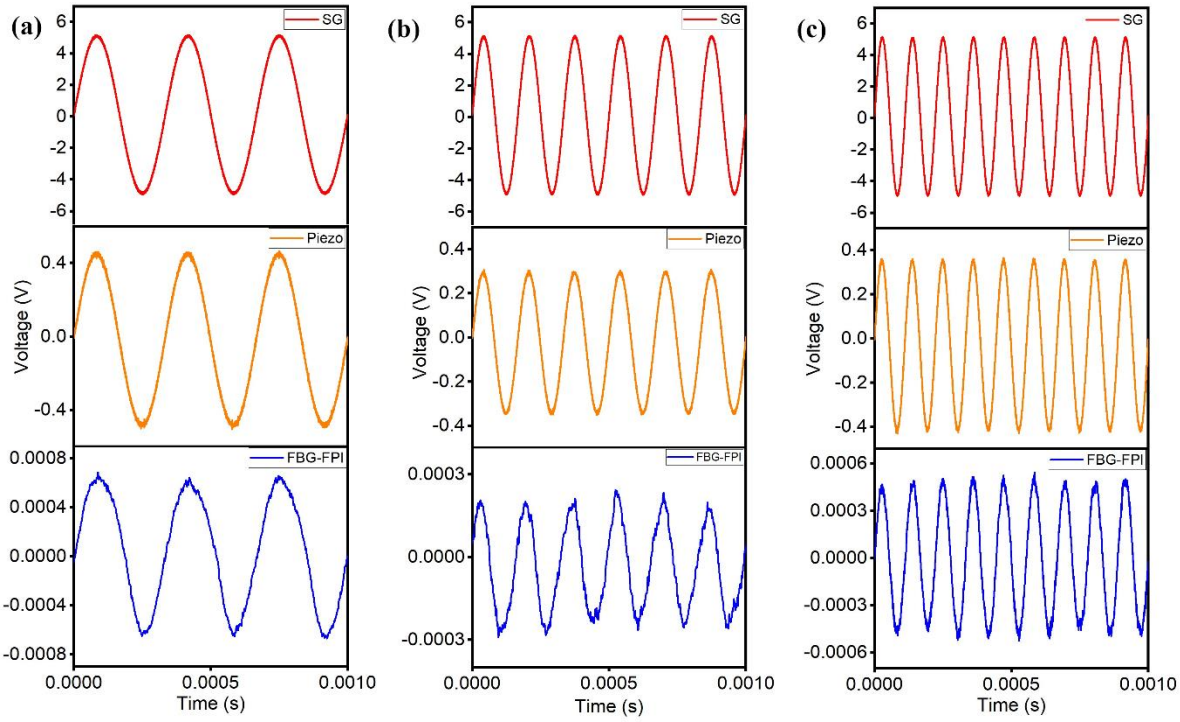

Fig. 9. Output signal comparison between the signal generator (SG – in red), the piezoelectric sensor (Piezo – in orange), and the FBG-FPI sensor (FBG-FPI in blue) for three different frequencies (a) 3 kHz, (b) 6 kHz, and (c) 9 kHz.

In order to ensure that compensation can be made for any temperature excursions, the FBG-FPI sensor was subjected to changes in the temperature, over the range from ~26°C (room temperature) to 80° C. The output spectra obtained during these tests were recorded at port 3 of the circulator using the OSA and Fig. 10a illustrates all the spectra obtained during the temperature rise to 80°C. It can be clearly seen that the sensor works well across this important temperature range as the FBG peak was always within the optimum operating range of the FPI (as the FBGs used in the FPI were placed closely together), enabling the FBG-FPI to always capture waveforms regardless of surrounding temperature changes. The characteristic wavelength of the FBG used in the FPI acts as a temperature sensor which can be calibrated, as shown in Fig 10b. [can you draw here a graph of the peak wavelength of the FBG v temperature using the peak wavelength data in Fig. 11a – upper graphs (from 30 deg to 80 deg) to show this? It should be linear and give that temperature calibration]

Fig. 11a shows the spectral responses of both the FBG (top) and the FPI (bottom) at a series of temperatures – 30, 40, 50, 60, 70, and 80°C showing that the wavelength shifts of the FBG themselves and of the FPI created were simultaneous and identical when they were subjected to the same temperature changes. Fig 11b shows the peak wavelength of the FPI created, as a function of temperature. [can you draw here a graph of the peak wavelength of

the FPI v temperature using the peak wavelength data in Fig. 11 – lower graphs (from 30 deg to 80 deg) to show this? It should be linear and give that calibration with temperature]

Thus Figs. 10 and 11 verify that temperature changes would not affect the ability of the FBG-FPI to capture burst and sine signals, as the reflective peak of the FBG is always within the FPI operating range over the temperature excursion range studied.

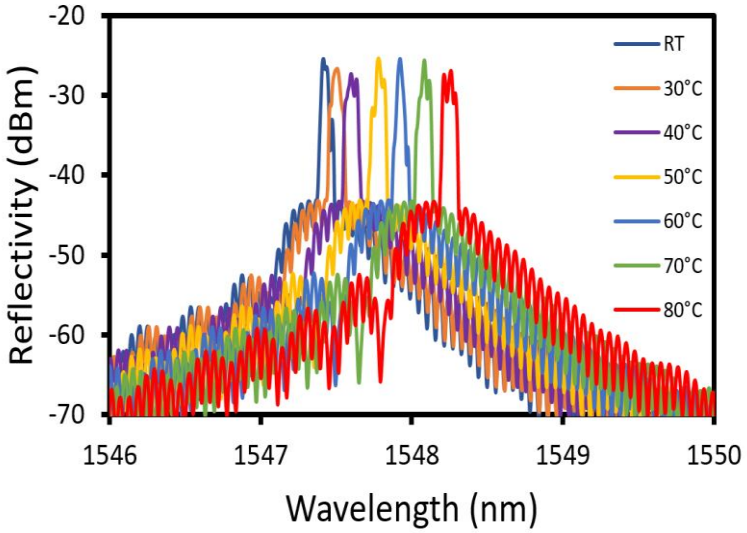

Fig. 10(a). Output spectra of the FBG-FPI when it is subjected to a different temperature.

[add Fig 10(b) – see above]

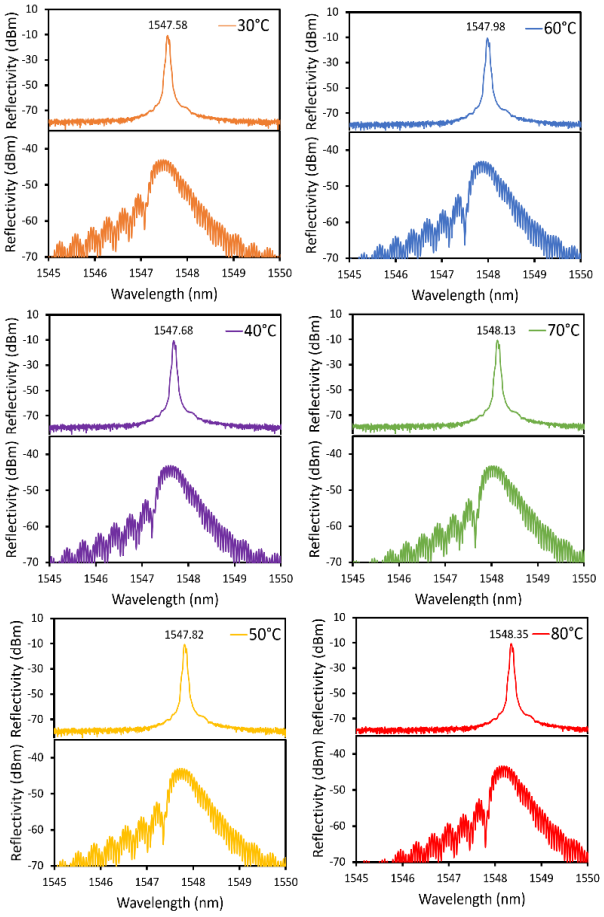

Fig. 11(a). Response spectra of each FBG and FPI at 30, 40, 50, 60, 70, and 80°C.

[add Fig 11(b) – see above]

Fig. 12 shows the FBG-FPI responses to a 3kHz burst at (a) 1 Hz, (b) 2 Hz, and (c) 3 Hz at room temperature (blue) and 80°C (red). It is clear from Fig. 11(a), that the FBG-FPI can capture the burst signal pattern, and so so over all the temperatures in the range shown. Further, similar response patterns can be observed for bursts at 2 Hz and 3 Hz in (b) and (c) respectively. This observation shows clearly that the method proposed is able to allow the FBG-FPI to detect burst signals, at these low frequencies, regardless of the temperature change.

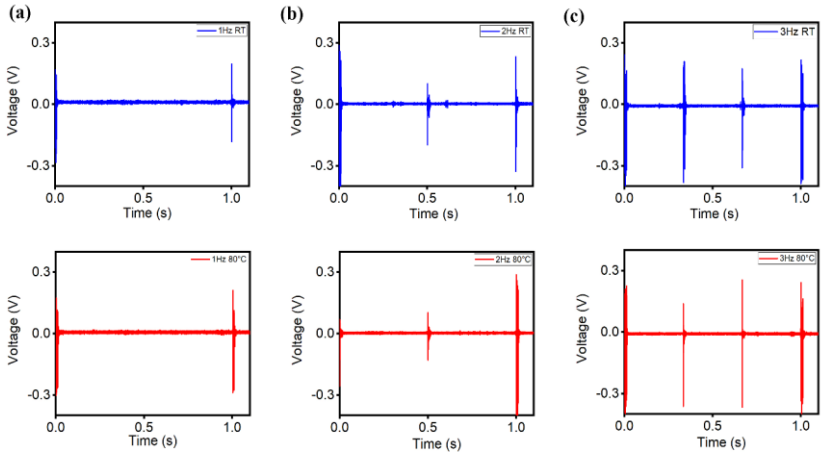

Fig. 12. The response of the FBG-FPI towards 3kHz bursts at (a) 1 Hz, (b) 2 Hz, and (c) 3 Hz intervals at room temperature (blue) compared to at 80°C (red).

In addition to that, the response of the FBG-FPI to any temperature changes in high-frequency sine waves can be observed in Fig. 13. Fig. 13 (a) shows the FBG-FPI was able to detect the 3 kHz sine waves at temperatures both of 40°C and 80°C and they exhibit similar responses towards temperature for frequencies of 6 kHz and 9 kHz, as shown in (b) and (c) respectively. There is also no observable difference in the amplitude response, whenever the FBG-FPI was subjected to different temperatures.

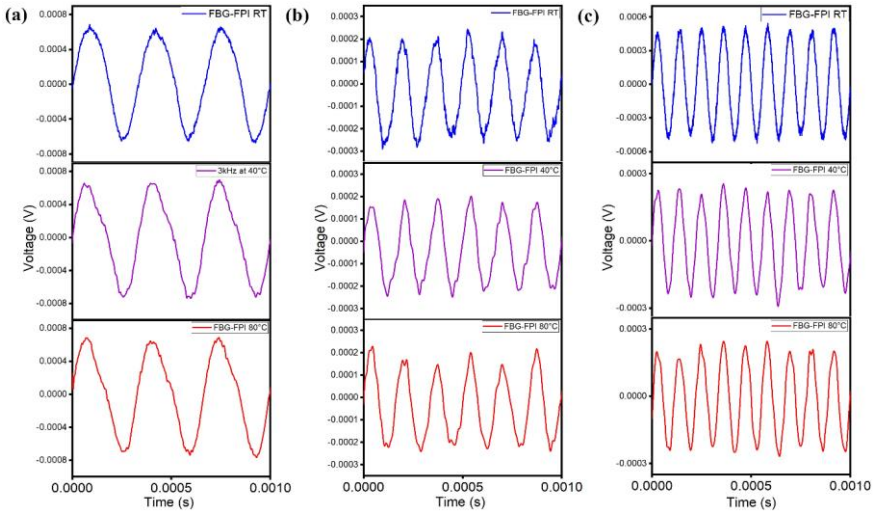

Fig. 13. The response of the FBG-FPI towards (a) 3 kHz, (b) 6 kHz and (c) 9 kHz sine waves at room temperature (blue), 40°C (purple) and 80°C (red).

4. Conclusions and Discussion

The research carried out has shown that a simple but highly effective, fiber FBG-FPI sensor has been developed and its performance verified, showing clearly that it is able to capture burst signals, in low-frequency intervals and sinusoidal waves in the high-frequency region of 3 kHz to 9 kHz, with high fidelity. Furthermore, due to the compactness of the design with the FBGs comprising the FPI being placed and aligned closely to each other, the sensor will still be effective over the important temperature range studied, because the effects of temperature on the peak of the reflected peak wavelength of the FBG and of the FPI formed from them are very closelty matched.

The design of the sensor has been carefully created so that the light source is always operating within the optimum wavelength range to suit the FPI operating as an interferometer, as well as matching the characteristic wavelengths of the FBGs themselves. Such a small, lightweight, all-optical and temperature-independent vibration sensor capable of detecting the waveforms of vibration over this frequency range opens up a variety of engineering applications, including in structural health monitoring (SHM) and ground movement monitoring amongst others, both particularly important in structural engineering today.

References

[1] A.P. Adewuyi, Z. Wu, N.H.M. Kammrujaman Serker, Assessment of vibration-based damage identification methods using displacement and distributed strain measurements, Struct. Heal. Monit. 8 (2009) 443–461. https://doi.org/10.1177/1475921709340964.

[2] Z. Abas, D.H. Yang, H.S. Kim, M.K. Kwak, J. Kim, Characterization of Electro-Active Paper Vibration Sensor by Impact Testing and Random Excitation, Int. J. Appl. Mech. 7 (2015) 1–18. https://doi.org/10.1142/S1758825115500659.

[3] S. Tadigadapa, K. Mateti, Piezoelectric MEMS sensors: State-of-the-art and perspectives, Meas. Sci. Technol. 20 (2009). https://doi.org/10.1088/0957-0233/20/9/092001.

[4] H.-C. Lee, W.-H. Bae, Study on the Elimiation of Irreversible Magnetic Components Using Anhysteretization in a Magnetostrictive Vibration Sensor, Trans. Korean Soc. Noise Vib. Eng. 20 (2010) 841–848. https://doi.org/10.5050/ksnve.2010.20.9.841.

[5] C.T. Chiang, C.I. Chang, W. Fang, Design of a digitized vibration detector implemented by CMOS digitized capacitive transducer with in-plane SoI accelerometer, IEEE Sens.

J. 14 (2014) 2546–2556. https://doi.org/10.1109/JSEN.2014.2303646.

[6] X. Liu, B. Jin, Q. Bai, Y. Wang, D. Wang, Y. Wang, Distributed fiber-optic sensors for vibration detection, Sensors (Switzerland). 16 (2016). https://doi.org/10.3390/s16081164.

[7] P. Kishore, D. Dinakar, K. Srimannarayana, P. Vengal Rao, Vibration sensor using 2 × 2 fiber optic coupler, Opt. Eng. 52 (2013) 107104. https://doi.org/10.1117/1.oe.52.10.107104.

[8] Z. Zhang, X. Bao, Continuous and damped vibration detection based on fiber diversity detection sensor by Rayleigh backscattering, J. Light. Technol. 26 (2008) 832–838. https://doi.org/10.1109/JLT.2008.919446.

[9] N. Linze, P. Tihon, O. Verlinden, P. Mégret, M. Wuilpart, Development of a multi-point polarization-based vibration sensor, Opt. Express. 21 (2013) 5606. https://doi.org/10.1364/oe.21.005606.

[10] H. Ohno, H. Naruse, M. Kihara, A. Shimada, Industrial Applications of the BOTDR Optical Fiber Strain Sensor, Opt. Fiber Technol. 7 (2001) 45–64. https://doi.org/10.1006/ofte.2000.0344.

[11] J. Villatoro, V.P. Minkovich, D. Monzón-Hernández, Temperature-independent strain sensor made from tapered holey optical fiber, Opt. Lett. 31 (2006) 305. https://doi.org/10.1364/ol.31.000305.

[12] A. Masoudi, M. Belal, T.P. Newson, A distributed optical fibre dynamic strain sensor based on phase-OTDR, Meas. Sci. Technol. 24 (2013). https://doi.org/10.1088/0957-0233/24/8/085204.

[13] C. Li, B. Dong, S. Li, C. Song, Er3+-Yb3+ co-doped silicate glass for optical temperature sensor, Chem. Phys. Lett. 443 (2007) 426–429. https://doi.org/10.1016/j.cplett.2007.06.081.

[14] A. Irace, G. Breglio, All-silicon optical temperature sensor based on Multi-Mode Interference, Opt. Express. 11 (2003) 2807. https://doi.org/10.1364/oe.11.002807.

[15] Z. Zhang, X. Bao, Distributed optical fiber vibration sensor based on spectrum analysis of Polarization-OTDR system, Opt. Express. 16 (2008) 10240. https://doi.org/10.1364/oe.16.010240.

[16] J. Villatoro, E. Antonio-Lopez, A. Schülzgen, R. Amezcua-Correa, Miniature multicore optical fiber vibration sensor, Opt. Lett. 42 (2017) 2022. https://doi.org/10.1364/ol.42.002022.

[17] R. Sifta, P. Munster, P. Sysel, T. Horvath, V. Novotny, O. Krajsa, M. Filka, Distributed

fiber-optic sensor for detection and localization of acoustic vibrations, Metrol. Meas. Syst. 22 (2015) 111–118. https://doi.org/10.1515/mms-2015-0009.

[18] H. J. Bang, S.M. Jun, C.G. Kim, Stabilized interrogation and multiplexing techniques for fibre Bragg grating vibration sensors, Meas. Sci. Technol. 16 (2005) 813–820. https://doi.org/10.1088/0957-0233/16/3/024.

[19] T.C. Liang, Y.L. Lin, Ground vibrations detection with fiber optic sensor, Opt. Commun. 285 (2012) 2363–2367. https://doi.org/10.1016/j.optcom.2012.01.037.

[20] L. Lu, Z. Cao, J. Dai, F. Xu, B. Yu, Self-mixing signal in Er 3+-Yb 3+ codoped Distributed Bragg Reflector fiber laser for remote sensing applications up to 20 Km, IEEE Photonics Technol. Lett. 24 (2012) 392–394. https://doi.org/10.1109/LPT.2011.2179922.

[21] L. Lu, J. Yang, Y. Zhao, Z. Du, B. Yu, Self-mixing interference in an all-fiberized configuration Er 3+-Yb 3+ codoped distributed Bragg reflector laser for vibration measurement, Curr. Appl. Phys. 12 (2012) 659–662. https://doi.org/10.1016/j.cap.2011.09.018.

[22] C. Wang, Y. Zhou, H. Dong, M. Tang, S. Fu, P. Shum, Quasi-distributed fiber sensor based on Fresnel-reflection-enhanced Incomplete-POTDR system, 24th Int. Conf. Opt. Fibre Sensors. 9634 (2015) 96347F. https://doi.org/10.1117/12.2194481.

[23] M. Ren, P. Lu, L. Chen, X. Bao, Theoretical and Experimental Analysis of Φ-OTDR Based on Polarization Diversity Detection, IEEE Photonics Technol. Lett. 28 (2016) 697–700. https://doi.org/10.1109/LPT.2015.2504968.

[24] Y. Muanenda, C.J. Oton, S. Faralli, F. Di Pasquale, A Cost-Effective Distributed Acoustic Sensor Using a Commercial Off-the-Shelf DFB Laser and Direct Detection Phase-OTDR, IEEE Photonics J. 8 (2016) 1–10. https://doi.org/10.1109/JPHOT.2015.2508427.

[25] Q. Zhang, T. Zhu, Y. Hou, K.S. Chiang, All-fiber vibration sensor based on a Fabry–Perot interferometer and a microstructure beam, J. Opt. Soc. Am. B. 30 (2013) 1211. https://doi.org/10.1364/josab.30.001211.

[26] N. Sathitanon, S. Pullteap, A Fiber Optic Interferometric Sensor for Dynamic Measurement, Int. J. Mech. Mechatronics Eng. 1 (2007) 667–670. https://doi.org/10.5281/zenodo.1061607.

[27] G. Giuliani, M. Norgia, S. Donati, T. Bosch, Laser diode self-mixing technique for sensing applications, J. Opt. A Pure Appl. Opt. 4 (2002). https://doi.org/10.1088/1464-4258/4/6/371.

[28] A. Chijioke, J. Lawall, Laser Doppler vibrometer employing active frequency feedback, Appl. Opt. 47 (2008) 4952–4958. https://doi.org/10.1364/AO.47.004952.

[29] P. Castellini, M. Martarelli, E.P. Tomasini, Laser Doppler Vibrometry: Development of advanced solutions answering to technology's needs, Mech. Syst. Signal Process. 20 (2006) 1265–1285. https://doi.org/10.1016/j.ymssp.2005.11.015.

[30] H.F. Lima, R. Da Silva Vicente, R.N. Nogueira, I. Abe, P.S. De Brito André, C. Fernandes, H. Rodrigues, H. Varum, H.J. Kalinowski, A. Costa, J. De Lemos Pinto, Structural health monitoring of the church of santa casa da misericórdia of Aveiro using FBG sensors, IEEE Sens. J. 8 (2008) 1236–1242. https://doi.org/10.1109/JSEN.2008.926177.

[31] U. Tiwari, V. Mishra, S.C. Jain, K. Kesavan, K. Ravisankar, N. Singh, G.C. Poddar, P. Kapur, Health monitoring of steel and concrete structures using fibre Bragg grating sensors, Curr. Sci. 97 (2009) 1539–1542.

[32] A. Wada, S. Tanaka, N. Takahashi, High-sensitivity vibration sensing using in-fiber Fabry-Perot interferometer with fiber-Bragg-grating reflectors, 20th Int. Conf. Opt. Fibre Sensors. 7503 (2009) 75033L. https://doi.org/10.1117/12.834166.

[33] A. Wada, S. Tanaka, N. Takahashi, Optical fiber vibration sensor using FBG Fabry-Perot interferometer with wavelength scanning and fourier analysis, IEEE Sens. J. 12 (2012) 225–229. https://doi.org/10.1109/JSEN.2011.2141984.

[34] R. YJ, H. PJ, J. DA, Z. L., B. I., Simultaneous strain, temperature and vibration measurement using a multiplexed in-fibre-Bragg-grating/fibre-Fabry-Perot sensor system, Electron. Lett. 33 (1997) 2063-2064(1). https://digital-library.theiet.org/content/journals/10.1049/el_19971409.

[35] M. K. A. Zaini, Y.S. Lee, N. Ismail, K.S. Lim, W. Udos, M.H. Zohari, H.Z. Yang, H. Ahmad, In-fiber Fabry Perot interferometer with narrow interference fringes for enhanced sensitivity in elastic wave detection, Opt. Fiber Technol. 53 (2019). https://doi.org/10.1016/j.yofte.2019.102021.